Soft Matter

Accepted Manuscript

This article can be cited before page numbers have been issued, to do this please use: Y. Zhuo, T. Li, F. Wang, V. Håkonsen, S. Xiao, J. He and Z. Zhang, *Soft Matter*, 2019, DOI: 10.1039/C9SM00162J.

ROYAL SOCIETY OF CHEMISTRY

rsc.li/soft-matter-journal

ROYAL SOCIETY OF CHEMISTRY
View Article Online
DOI: 10.1039/C9SM00162J

Soft Matter

ARTICLE

Ultra-durable Icephobic Coating by Molecular pulley

Yizhi Zhuo, Tong Li, Feng Wang, Verner Håkonsen, Senbo Xiao, Jianying He and Zhiliang Zhang**

Received 00th January 20xx,
Accepted 00th January 20xx

DOI: 10.1039/x0xx00000x

www.rsc.org/

Slide-ring crosslinked polydimethylsiloxane (PDMS) is designed and prepared for anti-icing/deicing application. Compared with the covalent crosslinks, the slidable crosslinks enhance the mobility of polymer networks and endow the materials with low elastic modulus. PDMS matrix guarantees the hydrophobicity of as-prepared coatings. These properties synergistically lead to ultra-low ice adhesion strength (13.0±1.3 kPa) and excellent mechanical durability. The ice adhesion strength on the coating maintains at a value of ~12 kPa during 20 icing/deicing cycles, and increases gradually to a value of ~22 kPa after 800 cycles of abrasions. The novel design strategy provides one-step forward to anti-icing/deicing solutions for targeted applications.

Introduction

Surfaces with low adhesion to ice has been widely investigated in the last decade due to their ability to mitigate the severe effects associated with ice accretion.[1-10] Although tremendous efforts have been made to develop low ice adhesion surfaces, there were only a few types of surfaces that can reach the value of ice adhesion strength below 20 kPa. The bioinspired slippery liquid-infused porous surface (SLIPS) is one of them, presenting ultra-low ice adhesion strength owing to the liquid lubricating film at the interface between the ice and the underlying porous substrate.[11, 12] Unfortunately, the SLIPS was found to be nondurable because of the high mobility of the liquid lubricant, which is easily removed by water or ice.[13] Soft coatings provide another type of surfaces that can obtain ice adhesion below 20 kPa. When external force is applied, these coatings can deform followed by generation of voids at the interface.[14, 15] These formed voids serve as crack initiators to facilitate the detachment of ice. So far, several soft coatings have demonstrated super-low adhesion to ice, and held encouraging promise for practical anti-icing/deicing applications.[1, 14, 16-19]

The separation of ice from coatings or substrates, in essence, is an interfacial fracture process. The maximum ice shear adhesion strength is governed by $\tau = \sqrt{EG/(\pi a \Lambda)}$, where *E, G, a* and *Λ* are the elastic modulus, surface energy, crack length and a non-dimensional constant related to geometric configuration, and in some cases the geometrical contribution $a\Lambda$ can be replaced by coating thickness *t*.[15, 20] Golovin et al[16] lowered the shear modulus of soft coatings by tailoring crosslinking density, and thus enabled interfacial slippage to reduce ice adhesion strength. Their icephobic surfaces showed very low ice adhesion below 10 kPa. Beemer el al[14] tuned the shear modulus and the thickness of the polydimethylsiloxane (PDMS) organogel to reach an ultra-low ice adhesion strength of 5.2 kPa. Very recently, our group introduced macroscale crack initiator (MACI) mechanism that incorporates sub-surface structures into PDMS to facilitate the formation of cracks at the interface, achieving a super-low ice adhesion strength of 5.7 kPa.[17] We further prepared sandwich-like PDMS, in which the ultra-low apparent elastic modulus guarantee a low ice adhesion strength down to 0.9 kPa, without using any surface additives.[18] It is noteworthy that all these coatings require deformation during the deicing process, which implies low elastic modulus is essential for reducing ice adhesion. In the above-mentioned studies, the elastic modulus of materials was often manipulated by decreasing their crosslinking density in the polymer matrix. However, low crosslinking density can effectively decrease the cohesive strength of material.[21, 22] In order to demonstrate that, PDMS coating with low crosslinking density was prepared by curing commercial Sylgard 184 with a weight ratio of 30/1 (base/curing agent). As shown in the insert image in Fig. 1a, cohesive failure occurred in such a coating (thickness: ~300 μm) during deicing, led to the loss of the structural integrity and durability. Hence, developing coatings with low elastic modulus, without simultaneous loss of cohesive strength, is crucial for durable anti-icing/deicing application.

Slide-ring materials, which is supramolecular crosslinked networks of polyrotaxane (Fig. 1a), have recently received attention because of their unique mechanical properties.[23-25] The topological interlocked architecture of slide-ring materials allows the molecular rings to slide along the backbone string easily, serving as a pulley at the nanoscale, and thus yielding a low Young's modulus in comparison with the traditional crosslinked polymer in same crosslinking density.[26] Furthermore, slide-ring material coatings present good scratch-resistance because of the elasticity and flexibility.[27] It can be expected that slide-ring materials with properly designed

NTNU Nanomechanical Lab, Department of Structural Engineering, Norwegian University of Science and Technology (NTNU), Trondheim 7491, Norway. E-mail: jianying.he@ntnu.no; zhiliang.zhang@ntnu.no

† Electronic Supplementary Information (ESI) available. See DOI: 10.1039/x0xx00000x

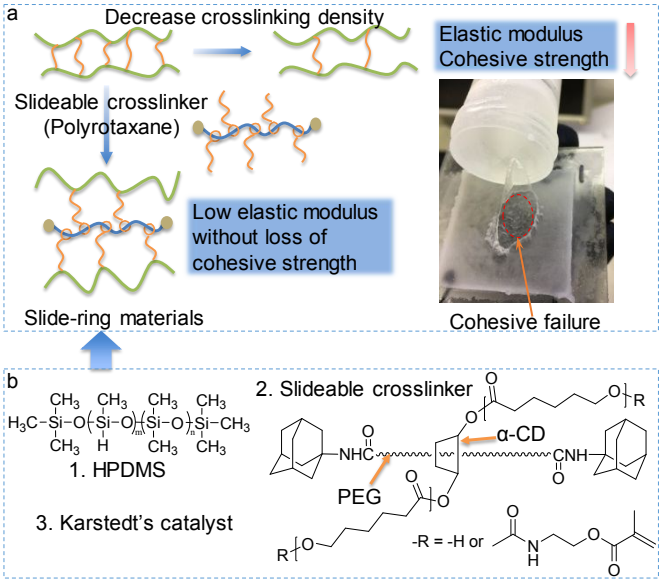

Fig. 1 (a) Comparison of low crosslinked polymer and slide-ring materials (insert image is cohesive failure of Sylgard 184 with a base/curing agent weight ratio of 30/1). (b) Synthesis of slide-ring PDMS: HPDMS react with vinyl-functionalized slideable crosslinker in the presence of Karstedt's catalyst to form polymeric networks.

molecular structure can serve as a candidate for durable anti-icing/deicing applications.

Herein, we prepared slide-ring PDMS (SP) through the crosslinking reaction of methylhydrosiloxane-dimethylsiloxane copolymer (HPDMS) with vinyl-functionalized polyrotaxane (slidable crosslinker, SA3403P), as shown in Fig. 1b, more detail can be found in experimental section. SA3403P consists of a backbone string (polyethylene glycol chain, PEG), rings (vinyl-functionalized α-cyclodextrin, α-CD), and two bulky end groups (adamantane). In the presence of Karstedt's catalyst, the Si-H bonds in HPDMS react with the vinyl groups that attached to the rings (α-CD) of polyrotaxane. The ATR-FTIR spectra of SP are shown in Fig. S1. Since there are no covalent bonds between HPDMS chain and the thread (PEG chain), or between the thread and the rings, the rings coupled to the HPMDS chains can move freely along the thread, thus serving as a moving pulley to lower the elastic modulus. The large free volume and flexible chains of crosslinked HPDMS also ensure the low modulus of the prepared coating. In addition, HPDMS possesses low surface energy, which is also one of the requirements for low ice adhesion of soft coatings. We tuned the crosslinking density of SP, denoted as SP-5%, SP-10%, and SP-15% (the percentages are the weight ratio of SA3404P and HPDMS), and characterized their surface topography, dynamic contact angle, mechanical properties, and anti-icing/deicing properties. The results were then used to establish the relationship between crosslinking density, properties, and ice adhesion strength of the new durable icephobic materials with molecular pulley.

Experimental section

Materials

(0.5-1.5% Methylhydrosiloxane)-dimethylsiloxane copolymer (HPDMS, trimethylsiloxane terminated, 5000-8000 cst) and Karstedt's catalyst (Platinum-divinyltetramethyldisiloxane complex in xylene) were purchased from Gelest. Toluene was obtained from Sigma-Aldrich. Vinyl-functionalized polyrotaxane (SA3403P) was supplied by Advanced Soft Materials (Kashiwa, Japan), and was used without further purification.

Fabrication

To 15 mL toluene, 3.0 g HPDMS and x g (x = 0.15, 0.30, or 0.45) SA3404P were added and mixed by VWR mixer for 3 min. Afterwards, 30 µL of Platinum-divinyltetramethyldisiloxane complex in xylene was added into the mixture, and mixed by VWR mixer for another 2 min. Then 5 mL of the resulting solution was poured onto the home-made mold. The mold was keept at room temperature to allow the evaporation of solvent, followed by cured at 80 °C for 24 h. The formed coatings were termed as SP-5%, SP-10% and SP-15%, where SP denote slide-ring PDMS, and the percentages are the weight ratio of SA3404P and HPDMS.

Characterization

Attenuated total reflectance-Fourier transform infrared (ATR-FTIR) spectrum of the samples were characterized on a ATR-FTIR spectrometer (Thermo Nicolet Nexus) under ambient conditions. Thermogravimetric Analysis (TGA) of the coatings were conducted on a thermogravimetric analyser (Netzsch TG 209F1 Libra) to evaluate the thermal stability. The samples were heated from 30 °C to 800 °C at a heating rate of 10 °C min^{-1} under a nitrogen atmosphere. Scanning electron microscopy (SEM) was conducted in a field emission scanning electron microscope (FEI APREO SEM) to characterize the surface morphology of the coatings. All samples were sputter-coated with a 10 nm gold layer before SEM characterization. Dynamic contact angles of deionized water on the samples were measured on a Drop Shape Analyzer (DSA100, KRÜSS). 10 µL of deionized water was expanded and shrunk on the sample via needle from the syringe. Mechanical properties were characterized by quasi-static nanoindentation tests (TriboIndenter 950, Hysitron, Inc.) by using a cylindrical diamond flat punch with 53.70 ± 0.06 µm diameter. The samples were loaded to the maximum load (75 µN) in 5 s, followed by holding for 2 s, then unloading for another 5 s. The unloading stiffness S of the samples was obtained from the slope of linear-fitting curve in the initial unloading part. The elastic modulus of coatings was approximated to $E = 0.75 * S/D$, where D is the dimeter of indenter, as shown in our previous paper.[1] Differential Scanning Calorimetry (DSC) experiments were performed using a Netzsch DSC (214 Polyma). The sample was placed into aluminum crucible and heated from -65 °C to 30 °C at a heating rate of 10 °C min^{-1}. Absolute digimatic indicator (Mitutoyo, ID-C112GB) was used to measure the thicknesses of the coatings. The thickness of SP was found to be 361±18 µm. The ice adhesion strength of samples and the sample during icing/deicing cycles was measured by vertical mode at -18 °C with a velocity of 0.01 mm s^{-1}, as shown in our previous report.[1] To evaluate the durability

during abrasion cycles, samples were abraded by 400-grit sandpaper at a pressure of 1.5 kPa with linear back-and-forth motion, and ice adhesion strengths of samples were recorded every 200 cycles.

Results and discussion

A micro-nano hierarchical surface topography is often a prerequisite for self-cleaning and water-repellent properties, seen in lotus leaf and other superhydrophobic surfaces.[28-33] However, for anti-icing/deicing applications, the surface texture may lead to mechanical interlocking, thus increasing the ice adhesion strength, especially under a high humidity environment.[2, 4, 34-36] Herein, the surface topography of SP was studied by scanning electron microscopy (SEM), as shown in Fig. S3. The smooth surfaces inhibit the mechanical interlocking between ice and the coatings. Dynamic water contact angles of SP was measured to evaluate surface energy that also affects the anti-icing/deicing properties. Fig. 2a and 2b show the advancing contact angle (Θ_{adv}) and receding contact angle (Θ_{rec}) of SP-15% as a representative. As shown in Fig. 2c, Θ_{adv} of three coatings with different content of SA3403P are nearly same, around 112°, while Θ_{rec} decreases from 88.7° to 76.8° with the increase of SA3403P content, and thus contact angle hysteresis ($\Delta\Theta=\Theta_{adv}-\Theta_{rec}$) increases with the increase of SA3403P content. This can be attributed to the dynamic rearrangement of amphiphilic SA3403P.[37, 38] The thread (PEG chain) of SA3403P is hydrophilic, while the functionalized rings (α-CD) are hydrophobic. The hydrophilic parts could bury themselves in the hydrophobic matrix tending to lower the surface energy in the air or the hydrophobic environment. However, they will rearrange themselves at the interface of coating and water once the coating is exposed to water, driven by the hydration energy, as shown in Fig. 2d. Hence, the surface with the most abundant SA3403P (SP-15%) shows the lowest Θ_{rec} and the largest $\Delta\Theta$.

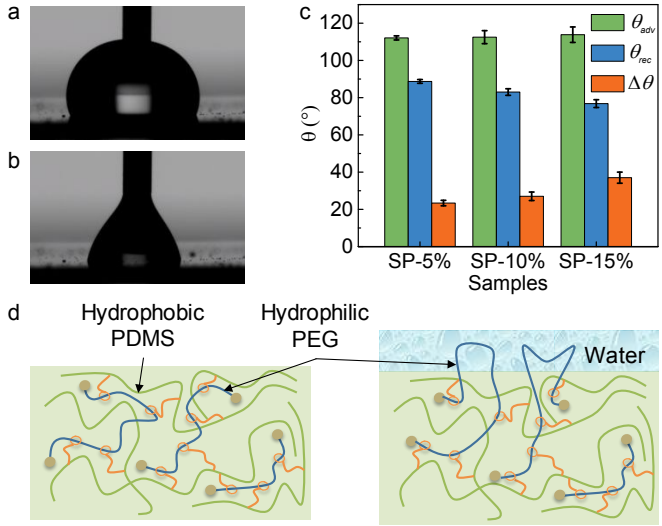

Fig. 2 Images of (a) advancing and (b) receding water contact angles of SP-15%. (c) Measured advancing (Θ_{adv}), receding (Θ_{rec}) water contact angles, and contact angle hysteresis ΔΘ of SP coatings, and (d) sketch for dynamic rearrangement of amphiphilic molecules.

The mechanical properties of the SPs were investigated by quasi-static nanoindentation with a flat punch indenter with diameter of 53 μm. There is no obvious hysteresis loop for all as-prepared SP in the load-depth curves shown in Fig. 3a, coinciding with previous results of other slide-ring materials.[23, 26] The rings are expected to be distributed randomly before loading and can move along with the string to approach each other during the mechanical loading. Once the loading is relieved, the rings return to their original state via entropic repulsion.[39, 40] The elastic modulus of the SPs was calculated from the fitting line of the initial unloading curve, where the calculation process can be found in the experimental section.[1, 41] Surprisingly, the elastic modulus of SP decrease from 0.40 to 0.26 MPa as the SA3403P content increases, as shown in Fig. 3b. Generally, the elastic modulus of crosslinked polymer increase with the content of crosslinker.[42] Herein, there are more than one vinyl group grafted on the rings. When two or more vinyl groups that are grafted on the same ring reacts with the Si-H bonds in HPDMS, covalent crosslinks can form, thus suppressing the pulley effect, as depicted in Fig. 3c. As the SA3403P content increases, vinyl groups become excessive, leading to the reduction of covalent crosslinks. As a result, SP-15% presents the lowest elastic modulus. Furthermore, differential scanning calorimetry (DSC) was conducted to examine the glass transition temperature (t_g) because temperature change may affect the elastic modulus of the material, especially around the t_g zone. Fortunately, the t_g of SP is well below -65 °C, according to the DSC curves shown in Fig. S4 (there is no signal of glass transition temperature in the measured range from -65 °C to 30 °C). This means that SP can remain in an elastomeric state down to -65 °C, and it would not have a big change in the elastic modulus at the temperature range of -65 to 30 °C.

Ice on the surfaces with a sufficiently low adhesion strength can be removed by natural forces, such as wind shear or its own gravity.[43] Herein, ice adhesion strength of SPs was measured by vertical shear test.[1, 17, 44] SP-5%, SP-10%, and SP-15% present ice adhesion strength of 13.8±2.1, 13.0±1.3, and 16.2±2.1 kPa, respectively (Fig. 4a). The thickness of SP coating was found to

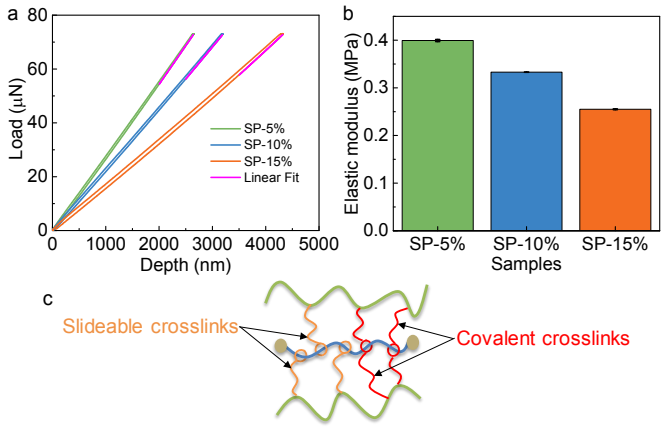

Fig. 3 (a) The load-depth curves of SP by flat punch nanoindentation, (b) elastic modulus of SP calculated from the load-depth curves, and (c) molecular schematic of slidable crosslinks and covalent crosslinks.

View Article Online
DOI: 10.1039/C9SM00162J

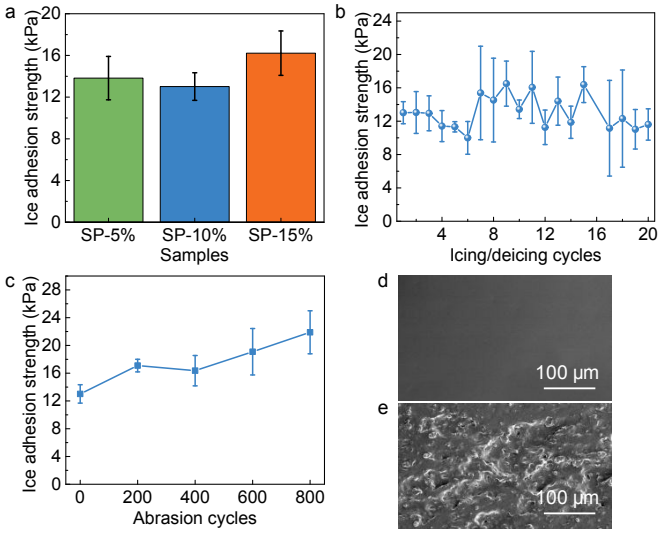

Fig. 4 (a) Ice adhesion strength of SP measured by vertical shear testing method, (b) ice adhesion strength of SP-10% during icing/deicing cycles, (c) ice adhesion strength of SP-10% as a function of abrasion cycles. SEM images of SP-10% (d) after 20 icing/deicing cycles, and (e) after 800 abrasion cycles.

be 361±18 μm. The ultra-low ice adhesion of SPs can be attributed to a combination of their low modulus resulted from the molecular pulley effect, and their hydrophobicity. The slidable molecules at the surface may also contribute to the low adhesion to ice, since they enable slippage effects similar to the interfacial slippage as Golovin *et al* proposed.[16] According to the classic theory of fracture mechanics, the maximum ice adhesion strength is governed by $\tau = \sqrt{EG/(\pi a \Lambda)}$. Besides, G equals to the practical work of adhesion, which is proportional to $(1 + \cos \theta_{rec})$.[45] Therefore, ice adhesion strength of such coating decreases with decreasing E and increasing Θ_{rec}. As a result, SP-10% shows lower ice adhesion strength, since it possesses lower elastic modulus in comparison with SP-5%, and larger Θ_{rec} in comparison with SP-15%. To evaluate the mechanical durability of SP, ice adhesion strengths of SP-10% during icing/deicing cycles and sandpaper abrasion cycles (see experimental section) were carried out. SP-10% retains its ultra-low ice adhesion strength at ~12 kPa during 20 icing/deicing cycles (Fig. 4b). As shown in Fig. 4c, the ice adhesion strength of SP-10% during the abrasion test was measured every 200 cycles. The adhesion strength value on the coating gradually increased to ~22 kPa after 800 abrasion cycles, which suggested that the coating possessed ultra-durable icephobicity for extreme wearing environment. To further demonstrate the mechanical durability of SP-10%, SEM imaging was performed after all of the icing/deicing cycles and abrasion cycles. As shown in Fig. 4d, the coating (SP-10%) after 20 icing/deicing cycles was found to be smooth and compact without any signs of damage. This indicates that during the icing/deicing cycles our SP coating can stay intact without cohesive failure, as previously shown in Scheme 1. The stable ice adhesion strength during icing/deicing tests is the result of durable structural integrity of coatings. In contrast, the surface of SP-10% after 800 abrasion cycles became uneven and rough (Fig. 4e), leading to the increase of ice adhesion strength. The reduction of coating thickness after abrasion could also contribute to the increase of ice adhesion strength. However, because the coating is soft and easy to deform with the deicing stress, the ice adhesion strength after 800 abrasion cycles is around 22 kPa, still significantly lower than previously reported durable anti-icing/deicing surfaces.[3] Overall, our coating shows ultra-low ice adhesion strength and excellent mechanical durability simultaneously.

Conclusions

In summary, motivated by interfacial fracture mechanics, we introduced the molecular pulley to PDMS matrix to prepare mechanically durable icephobic materials. The results show that the coating with the suitable content of slidable crosslinker (SP-10%) displays optimal surface energy and elastic modulus, and thus lowest ice adhesion strength. Notably, SP-10% presents excellent mechanical durability, maintaining an ultra-low ice adhesion strength of ~12 kPa during 20 icing/deicing cycles. Even after 800 abrasion cycles, it still remains at a very low value of ~22 kPa. This work sheds new light on the molecular design and fabrication of anti-icing/deicing materials with ultra-durability that can meet practical applications such as in wind turbine, aircraft and many others.

Conflicts of interest

There are no conflicts to declare.

Acknowledgements

The authors gratefully acknowledge the support of Research Council of Norway by PETROMAKS2 Project Durable Arctic Icephobic Materials (Project No. 255507) and the Norwegian Micro- and Nano-Fabrication Facility, NorFab, project number 245963.

Notes and references

1. Y. Zhuo, V. Hakonsen, Z. He, S. Xiao, J. He and Z. Zhang, *ACS Appl Mater Interfaces*, 2018, **10**, 11972-11978.
2. M. J. Kreder, J. Alvarenga, P. Kim and J. Aizenberg, *Nature Reviews Materials*, 2016, **1**, 15003.
3. Y. Wang, X. Yao, S. Wu, Q. Li, J. Lv, J. Wang and L. Jiang, *Adv Mater*, 2017, **29**.
4. H. Sojoudi, M. Wang, N. D. Boscher, G. H. McKinley and K. K. Gleason, *Soft Matter*, 2016, **12**, 1938-1963.
5. D. Chen, M. D. Gelenter, M. Hong, R. E. Cohen and G. H. McKinley, *ACS Appl Mater Interfaces*, 2017, DOI: 10.1021/acsami.6b13773.
6. Y. Y. Wang, J. Liu, M. Z. Li, Q. J. Wang and Q. M. Chen, *Applied Surface Science*, 2016, **385**, 472-480.
7. S. A. Kulinich and M. Farzaneh, *Applied Surface Science*, 2009, **255**, 8153-8157.
8. C. Laforte and J.-L. Laforte, *Journal of Adhesion Science and Technology*, 2012, **26**, 603-620.

9. F. Wang, W. Ding, J. He and Z. Zhang, *Chemical Engineering Journal*, 2019, **360**, 243-249.
10. S. Zhang, J. Huang, Y. Cheng, H. Yang, Z. Chen and Y. Lai, *Small*, 2017, DOI: 10.1002/smll.201701867.
11. T.-S. Wong, S. H. Kang, S. K. Y. Tang, E. J. Smythe, B. D. Hatton, A. Grinthal and J. Aizenberg, *Nature*, 2011, **477**, 443-447.
12. P. Kim, T.-S. Wong, J. Alvarenga, M. J. Kreder, W. E. Adorno-Martinez and J. Aizenberg, *ACS Nano*, 2012, **6**, 6569-6577.
13. Y. Zhuo, F. Wang, S. Xiao, J. He and Z. Zhang, *ACS Omega*, 2018, **3**, 10139-10144.
14. D. L. Beemer, W. Wang and A. K. Kota, *J. Mater. Chem. A*, 2016, **4**, 18253-18258.
15. M. K. Chaudhury and K. H. Kim, *The European physical journal. E, Soft matter*, 2007, **23**, 175-183.
16. K. Golovin, S. P. Kobaku, D. H. Lee, E. T. DiLoreto, J. M. Mabry and A. Tuteja, *Sci Adv*, 2016, **2**, e1501496.
17. Z. He, S. Xiao, H. Gao, J. He and Z. Zhang, *Soft Matter*, 2017, **13**, 6562-6568.
18. Z. He, Y. Zhuo, J. He and Z. Zhang, *Soft Matter*, 2018, **14**, 4846-4851.
19. P. Irajizad, A. Al-Bayati, B. Eslami, T. Shafquat, M. Nazari, P. Jafari, V. Kashyap, A. Masoudi, D. Araya and H. Ghasemi, *Materials Horizons*, 2019, DOI: 10.1039/c8mh01291a.
20. H. Yao and H. Gao, *Journal of Computational and Theoretical Nanoscience*, 2010, **7**, 1299-1305.
21. X. Zhang, Y. Ding, G. Zhang, L. Li and Y. Yan, *International Journal of Adhesion and Adhesives*, 2011, **31**, 760-766.
22. H. Schonhorn and R. H. Hansen, *Journal of Applied Polymer Science*, 1967, **11**, 1461-1474.
23. D. Yang, F. Ge, M. Tian, N. Ning, L. Zhang, C. Zhao, K. Ito, T. Nishi, H. Wang and Y. Luan, *J. Mater. Chem. A*, 2015, **3**, 9468-9479.
24. A. Bin Imran, K. Esaki, H. Gotoh, T. Seki, K. Ito, Y. Sakai and Y. Takeoka, *Nat Commun*, 2014, **5**, 5124.
25. K. Ohmori, I. Abu Bin, T. Seki, C. Liu, K. Mayumi, K. Ito and Y. Takeoka, *Chem Commun (Camb)*, 2016, **52**, 13757-13759.
26. K. Ito, K. Kato and K. Mayumi, 2015, DOI: 10.1039/9781782622284-00044, 44-77.
27. Y. Noda, Y. Hayashi and K. Ito, *Journal of Applied Polymer Science*, 2014, **131**, n/a-n/a.
28. C. Peng, Z. Chen and M. K. Tiwari, *Nat Mater*, 2018, **17**, 355-360.
29. L. Wang, Q. Gong, S. Zhan, L. Jiang and Y. Zheng, *Adv Mater*, 2016, **28**, 7729-7735.
30. X. Gao and L. Jiang, *Nature*, 2004, **432**, 36-36.
31. W. Shi, L. Wang, Z. Guo and Y. Zheng, *Advanced Materials Interfaces*, 2015, **2**, 1500352.
32. P. Guo, Y. Zheng, M. Wen, C. Song, Y. Lin and L. Jiang, *Adv. Mater.*, 2012, **24**, 2642-2648.
33. W. Li and A. Amirfazli, *Soft Matter*, 2008, **4**, 462-466.
34. J. Chen, J. Liu, M. He, K. Li, D. Cui, Q. Zhang, X. Zeng, Y. Zhang, J. Wang and Y. Song, *Applied Physics Letters*, 2012, **101**, 111603.
35. B. Liu, K. Zhang, C. Tao, Y. Zhao, X. Li, K. Zhu and X. Yuan, *RSC Adv.*, 2016, **6**, 70251-70260.
36. S. Bengaluru Subramanyam, V. Kondrashov, J. Ruhe and K. K. Varanasi, *ACS Appl Mater Interfaces*, 2016, **8**, 12583-12587.
37. M. Inutsuka, N. L. Yamada, K. Ito and H. Yokoyama, *ACS Macro Letters*, 2013, **2**, 265-268.
38. K. Yanagi, N. L. Yamada, K. Kato, K. Ito and H. Yokoyama, *Langmuir*, 2018, DOI: 10.1021/acs.langmuir.8b00649.
39. S. Choi, T. W. Kwon, A. Coskun and J. W. Choi, *Science*, 2017, **357**, 279-283.
40. K. Ito, *Polymer Journal*, 2011, **44**, 38-41.
41. Z. X. Wang, A. A. Volinsky and N. D. Gallant, *Journal of Applied Polymer Science*, 2015, **132**, n/a-n/a.
42. C. Creton, *Macromolecules*, 2017, **50**, 8297-8316.
43. K. Golovin and A. Tuteja, *Science Advances*, 2017, **3**.
44. Z. W. He, E. T. Vagenes, C. Delabahan, J. Y. He and Z. L. Zhang, *Scientific Reports*, 2017, **7**.
45. A. J. Meuler, J. D. Smith, K. K. Varanasi, J. M. Mabry, G. H. McKinley and R. E. Cohen, *ACS Applied Materials & Interfaces*, 2010, **2**, 3100-3110.

View Article Online
DOI: 10.1039/C9SM00162J

Table of contents:

Graphic abstract:

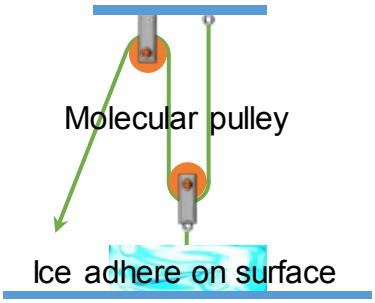

Highlight:

Molecular pulley have been designed and fabricated to mitigate ice accretion.